INTERNATIONAL TABLES FOR CRYSTALLOGRAPHY

ISSN 1574-8707
it.iucr.org

Volume I, X-ray Absorption Spectroscopy and Related Techniques
ISBN: 978-1-119-43394-1

Chapter 2.14

Keywords: EXAFS; thermal expansion; Debye–Waller factors.

Thermal effects on EXAFS

Paolo Fornasini*

Department of Physics, University of Trento, Via Sommarive 14, 38123 Trento-Povo, Italy. *Correspondence e-mail: paolo.fornasini@unitn.it

The effects of weak atomic vibrations on extended X-ray absorption fine-structure (EXAFS) spectra are discussed from a phenomenological perspective. Attention is focused on single-scattering paths and in particular on the first-shell contribution, in terms of bond expansion, parallel and perpendicular mean-square relative displacements, and distribution asymmetry. The main differences with respect to Bragg diffraction are stressed. Some theoretical methods that have been developed to simulate thermal effects on EXAFS are reviewed.

1. Introduction

A single photoelectron, with a time of flight ($\sim 10^{-16}$ s) much shorter than the period of atomic vibrations ($\sim 10^{-12}$ s), samples an instantaneous scattering path length. An EXAFS spectrum resulting from the behaviour of a large number of photoelectrons is the sum of the contributions of all relevant single-scattering (SS) and multiple-scattering (MS) paths, $\chi(k) = \sum_{\rm path} \langle \chi_{\rm path}(k) \rangle$, where $\langle \ldots \rangle$ represents the average over all possible vibrational and structural configurations for each path.

In practice, the most common approach consists of considering the photoelectrons as sampling a one-dimensional distribution $\rho_{\rm path}(r)$ of lengths for each scattering path. The position, width and shape of the $\rho(r)$ distributions depend on the intensity of the zero-point and thermal vibrational motion of atoms, and can be modified by the presence of structural disorder.

The damping of the EXAFS spectra $\chi(k)$ resulting from the effect of vibrational and structural disorder has been taken into account in the harmonic approximation through a Debye–Waller-like factor $\exp(-2k^2\sigma^2)$ since the initial pioneering work (Sayers *et al.*, 1971; Stern *et al.*, 1975, 1980; Ashley & Doniach, 1975; Lee & Pendry, 1975; Gurman & Pendry, 1976), where the factor σ^2 corresponds to the variance of a Gaussian distribution $\rho(r)$.

The limits of the harmonic approximation were discovered quite early on (Eisenberger & Brown, 1979), leading to more refined expressions for $\rho(r)$ corresponding to peculiar physical models (Boyce *et al.*, 1977; Crozier & Seary, 1980; Crozier *et al.*, 1988; Filipponi & Di Cicco, 1995). For relatively small degrees of thermal and structural disorder, the EXAFS function can be parametrized in terms of the leading cumulants of the distribution of distances (Bunker, 1983; Crozier *et al.*, 1988), with the second cumulant corresponding to the harmonic Debye–Waller exponent σ^2.

In this chapter, attention is focused on the effects of thermal disorder (including zero-point vibrations) on the single-scattering paths and on its treatment by the cumulant approach. A thorough understanding of thermal effects on

Related chapters

Volume I: 2.2, 3.29, 3.30, 5.11, 5.14

EXAFS can facilitate data-analysis procedures and the detection of structural disorder, provide original information on the local dynamics and clarify the meaning of the structural parameters obtained from EXAFS, in particular in comparison with Bragg diffraction.

2. Distributions and cumulants

The EXAFS signal for a single-scattering path (one coordination shell) is expressed, within the plane-wave approximation, as (Stern *et al.*, 1975; Crozier *et al.*, 1988)

$$\chi(k) = \frac{S_0^2}{k} N \,\mathrm{Im}\left[f(k,\pi) \exp(2i\delta) \int_0^\infty P(r,\lambda) \exp(2ikr)\, \mathrm{d}r \right]. \quad (1)$$

Here, $P(r,\lambda) = \rho(r)\exp(-2r/\lambda)/r^2$ is an effective distribution of distances which takes into account the decreasing ability of the photoelectron to sample the real distribution $\rho(r)$ as the distance r increases, owing to the effect of both the spherical nature of its wavefunction and the finite mean free path λ. If curved-wave effects are non-negligible, the scattering amplitude also weakly depends on r, and $f(k,\pi,r)$ should be taken under the integral of equation (1). A thorough treatment of disorder effects on curved-wave EXAFS can be found in Brouder (1988).

The distribution of distances cannot be obtained by a simple Fourier transform of the EXAFS signal. For moderate degrees of disorder, the integral appearing in equation (1) can be expanded as a power series of the wavenumber k (Bunker, 1983),

$$\int_0^\infty P(r,\lambda) \exp(2ikr)\, \mathrm{d}r = \exp\left[\sum_{n=0}^\infty (2ik)^n C_n/n! \right],$$

where C_n are the cumulants of the effective distribution $P(r,\lambda)$. The EXAFS signal can be parametrized in terms of the cumulants of the effective distribution as

$$\begin{aligned} k\chi(k) = {} & S_0^2 |f(k,\pi)| N \\ & \times \exp(C_0 - 2C_2k^2 + 2C_4k^4/3 + \ldots) \\ & \times \sin(C_1k - 4C_3k^3/3 + \ldots). \end{aligned}$$

Odd and even cumulants characterize the phase and the amplitude of the EXAFS signal $\chi(k)$, respectively. The cumulant method is presented at some length in Fornasini (2024) and in Appendix 2 of Bunker (2010); there, the connection between the cumulants C_n of the effective distribution and the cumulants C_n^* of the real distribution is also established: in general, only the difference between the first cumulants C_1^* and C_1 is non-negligible, $C_1^* = C_1 + 2C_2(1/C_1 + 1/\lambda)$, and the corresponding transformation is included in most data-analysis packages. The strengths and limitations of the cumulant approach are also discussed in Fornasini (2024) and references therein.

In the following, we directly consider the cumulants of the real distribution. $C_1^* = \langle r \rangle$ and $C_2^* = \sigma^2 = \langle (r - \langle r \rangle)^2 \rangle$ are the mean and the variance of the real distribution $\rho(r)$, respectively. Higher order cumulants quantify the deviation of the distribution from the Gaussian shape; in particular, the third cumulant $C_3^* = \langle (r - \langle r \rangle)^3 \rangle$ characterizes the distribution asymmetry and the fourth cumulant C_4^* describes the symmetric deviations from the Gaussian shape. The values of the cumulants characterize the effect of atomic vibrations and possibly of structural disorder.

The effects of thermal and structural disorder on multiple-scattering (MS) paths have been taken into account by a number of researchers according to different approaches (Alberding & Crozier, 1983; Boland & Baldeschwieler, 1984; Benfatto *et al.*, 1989; Loeffen & Pettifer, 1996; Poiarkova & Rehr, 1999; Rehr & Albers, 2000).

3. The one-dimensional model

An EXAFS experiment samples a one-dimensional distribution of distances for each scattering path. In the one-dimensional model, the vibrational properties of the absorber–backscatterer atomic pair are connected to a pair potential energy, which is conveniently expanded in powers of the displacement $u = r - r_0$ with respect to the position r_0 of the potential minimum,

$$V(u) = k_0u^2/2 + k_3u^3 + k_4u^4 + \ldots \quad (2)$$

3.1. Distribution and pair potential

The distribution $\rho(r)$ is connected to the Hamiltonian $H = T + V(r)$ of the atomic pair by the quantum relation

$$\rho(r) = \mathrm{Tr}(wP_r) = \frac{1}{\sum_n \exp(-\beta E_n)} \sum_n |\varphi_n|^2 \exp(-\beta E_n),$$

where $w = \exp(-\beta H)/\mathrm{Tr}[\exp(-\beta H)]$ is the statistical density operator, $P_r = |r\rangle\langle r|$ are the projectors on the $|r\rangle$ states, E_n and φ_n are the Hamiltonian eigenvalues and eigenfunctions, respectively, and $\beta = 1/k_\mathrm{B}T$.

For sufficiently high temperatures, the classical approximation holds:

$$\rho(r) = \frac{\exp[-\beta V(r)]}{\int \exp[-\beta V(r)]\, \mathrm{d}r}.$$

3.2. Cumulants and pair potential

When, for weak vibrational disorder, the distribution of distances is characterized by its leading cumulants, it is useful to express the temperature dependence of the cumulants in terms of the force constants of the pair potential (equation 2).

In the classical approximation, the cumulants can be evaluated (Stern *et al.*, 1991) as

$$C_n^* = \langle A_n(T) \rangle = \frac{\int A_n(r) \exp[-\beta V(r)]\, \mathrm{d}r}{\int \exp[-\beta V(r)]\, \mathrm{d}r},$$

where $A_1 = r$, $A_2 = (r - \langle r \rangle)^2$ and so on. One finds

$$\delta C_1^*(T) = -\frac{3k_3}{k_0^2}k_{\rm B}T + \frac{3k_3}{k_0^4}(k_{\rm B}T)^2\left(32k_4 - \frac{45k_3^2}{k_0}\right) + \ldots,$$
$$C_2^*(T) = \frac{k_{\rm B}T}{k_0} + \frac{3}{k_0^3}\left(\frac{12k_3^2}{k_0} - 4k_4\right)(k_{\rm B}T)^2 + \ldots,$$
$$C_3^*(T) = -\frac{6k_3}{k_0^3}(k_{\rm B}T)^2 - \ldots,$$
$$C_4^*(T) = \frac{12}{k_0^4}\left(\frac{9k_3^2}{k_0} - 2k_4\right)(k_{\rm B}T)^3 + \ldots$$

To first order, the bond expansion δC_1^* and the second cumulant C_2^* linearly depend on temperature, and the third and fourth cumulants are proportional to T^2 and T^3, respectively. The classical approximation cannot reproduce the low-temperature behaviour, where quantum effects are non-negligible. It can however give significant results on the anharmonicity effects at relatively high temperatures (Tranquada & Ingalls, 1983; Dalba & Fornasini, 1997).

The quantum approach is based on a perturbative expansion of the density matrix, where the anharmonic terms are considered as a small perturbation to the harmonic Hamiltonian. This approach was first proposed by Frenkel & Rehr (1993) for the thermal expansion and the third cumulant. The second-order calculation of the first four cumulants was made by Yokoyama (1999) and an extension to higher orders has been made by Haug *et al.* (2008). We list here only the main results; for more details, see the original papers and the review by Fornasini & Grisenti (2015).

Let $\omega = (k_0/\mu)^{1/2}$, $\sigma_0^2 = \hbar/2\mu\omega$ and $z = \exp(-\beta\hbar\omega)$, where μ is the reduced mass. To first order, the bond expansion (in the one-dimensional model) is

$$\delta C_1^*(T) = -(3k_3\sigma_0^2/k_0)\,(1+z)/(1-z) + \ldots \qquad (3)$$

The second cumulant is

$$C_2^*(T) = \sigma_0^2\frac{1+z}{1-z} - \frac{12\,k_4\sigma_0^6}{\hbar\omega}\frac{(1+z)^2}{(1-z)^2} - \frac{24\,k_4\sigma_0^6}{k_{\rm B}T}\frac{z(1+z)}{(1-z)^3} + \frac{4k_3^2\sigma_0^8}{(\hbar\omega)^2}\frac{13z^2+58z+13}{(1-z)^2} + \frac{120k_3^2\sigma_0^8}{\hbar\omega k_{\rm B}T}\frac{z(1+z)}{(1-z)^3} + \ldots \qquad (4)$$

The first-order term corresponds to the harmonic approximation, where σ_0^2 is the zero-point value; the higher-order anharmonic contributions depend on k_3, k_4, ...

Again to first order, the third cumulant is

$$C_3^*(T) = -(2k_3\sigma_0^4/k_0)(z^2+10z+1)/(1-z)^2 - \ldots,$$

where $-2k_3\sigma_0^4/k_0$ is the zero-point value.

The fourth cumulant is

$$C_4^*(T) = -\frac{12\,k_4\sigma_0^8}{\hbar\omega}\frac{z^3+9z^2+9z+1}{(1-z)^3} - \frac{144k_4\sigma_0^8}{k_{\rm B}T}\frac{z^2}{(1-z)^4} + \frac{12\,k_3^2\sigma_0^{10}}{(\hbar\omega)^2}\frac{5z^3+109z^2+109z+5}{(1-z)^3} + \frac{720\,k_3^2\sigma_0^{10}}{\hbar\omega k_{\rm B}T}\frac{z^2}{(1-z)^4} + \ldots \qquad (6)$$

An example of the difference between the classical and quantum first-order approximations to the first three cumulants of the two-atomic molecule Br_2 is shown in Fig. 1.

By comparing equation (3) with the first terms of equations (4) and (5), one finds (Frenkel & Rehr, 1993) that, to first order, the ratio

$$a = -(3k_3/k_0)\,C_2 \qquad (7)$$

corresponds to the bond expansion δC_1^* of the one-dimensional model.

Only for two-atomic molecular gases does the one-dimensional model have a direct application (Stern *et al.*, 1979; Yokoyama *et al.*, 1996). For many-atomic molecules and condensed systems, the relationship between the three-dimensional structure and the one-dimensional model and its cumulants is not direct.

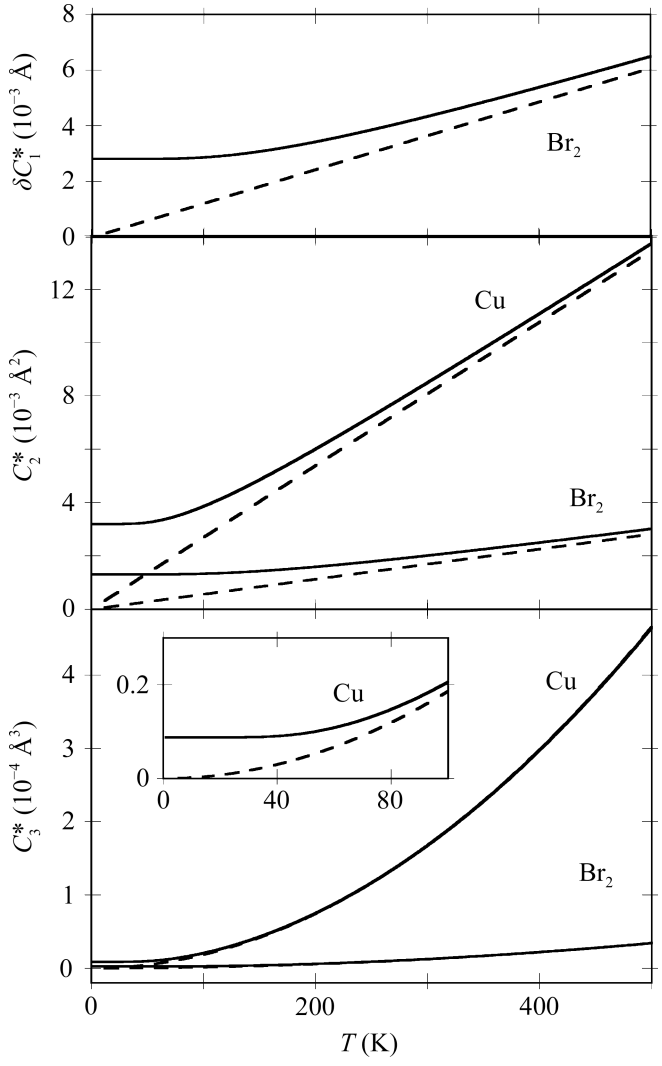

Figure 1
Temperature dependence of the first three cumulants of the Br_2 molecule and of the second and third cumulants of copper according to the equations in Section 3.2: first-order classical approximation (dashed lines) and first-order quantum approximation (continuous lines). The force constants are taken from Huber & Herzberg (1979) for Br_2 and from Fornasini *et al.* (2004) for copper.

3.3. Effective pair potential

In many-atomic systems, the distribution $\rho(r)$ can be affected by structural disorder, in addition to vibrational disorder. Even when only vibrational disorder is present, the potential energy $V(r)$ associated with the distribution $\rho(r)$ is an *effective* potential energy, which depends on the statistically averaged behaviour of all of the atoms of the system (Mustre de Leon *et al.*, 1992) and has to be distinguished both from the single-pair potential energy and from the total potential energy defined in a $3N$-dimensional configurational space.

3.4. Parallel mean-square relative displacement (MSRD)

To clarify the relation between the EXAFS cumulants and the vibrational properties of many-atomic systems, it is convenient to refer to the relative atomic displacements.

Let $\mathbf{R}$ be the distance between the average positions of the absorber and backscatterer atoms (a and b, respectively), and let $\mathbf{u}_a$ and $\mathbf{u}_b$ be their instantaneous displacements with respect to the average positions. The instantaneous interatomic distance $\mathbf{r}$ is

$$\mathbf{r} = \mathbf{R} + \mathbf{u}_b - \mathbf{u}_a = \mathbf{R} + \Delta\mathbf{u}.$$

It is convenient to consider the projection of the relative displacement $\Delta\mathbf{u}$ along the bond direction $\Delta u_\parallel$ and in the perpendicular plane $\Delta u_\perp$,

$$\Delta u_\parallel = \hat{\mathbf{R}} \cdot \Delta\mathbf{u}, \quad \Delta u_\perp^2 = \Delta u^2 - \Delta u_\parallel^2,$$

where the short-hand notations Δu^2 and $\Delta u_\parallel^2$ correspond to $(\Delta\mathbf{u})^2$ and $[\hat{\mathbf{R}} \cdot (\mathbf{u}_b - \mathbf{u}_a)]^2$, respectively.

For a single-scattering path, the second cumulant is

$$C_2^* = \sigma^2 = \langle (r - \langle r \rangle)^2 \rangle = (1/N) \sum_{b=1}^{N} \langle (r_b - \langle r_b \rangle)^2 \rangle,$$

where b labels the N backscattering atoms of the coordination shell. One can easily show that

$$C_2^* \simeq \langle \Delta u_\parallel^2 \rangle + \frac{1}{4R^2} \left\{ \langle \Delta u_\perp^4 \rangle - \left[\langle \Delta u_\perp^2 \rangle \right]^2 \right\},$$

where the leading contribution is the parallel MSRD $\langle \Delta u_\parallel^2 \rangle$; the second contribution is proportional to the variance of the distribution of the $\Delta u_\perp^2$ values and is generally negligible (Fornasini *et al.*, 2001).

The parallel MSRD can be decomposed as

$$\langle \Delta u_\parallel^2 \rangle = \langle (\hat{\mathbf{R}} \cdot \mathbf{u}_b)^2 \rangle + \langle (\hat{\mathbf{R}} \cdot \mathbf{u}_a)^2 \rangle - 2 \langle (\hat{\mathbf{R}} \cdot \mathbf{u}_b)(\hat{\mathbf{R}} \cdot \mathbf{u}_a) \rangle$$

(Beni & Platzman, 1976): the first two terms are the independent mean-square displacements, which can be calculated from the atomic displacement parameters of X-rays or neutron diffraction, while the third term depends on the correlation of the motion of absorber and backscatterer atoms. A convenient measure of correlation is (Booth *et al.*, 1995; Jeong *et al.*, 1999)

$$\varphi_\parallel(T) = \frac{\langle (\hat{\mathbf{R}} \cdot \mathbf{u}_b)^2 \rangle + \langle (\hat{\mathbf{R}} \cdot \mathbf{u}_a)^2 \rangle - \langle \Delta u_\parallel^2 \rangle}{2[\langle (\hat{\mathbf{R}} \cdot \mathbf{u}_b)^2 \rangle \langle (\hat{\mathbf{R}} \cdot \mathbf{u}_a)^2 \rangle]^{1/2}},$$

where $\varphi_\parallel = 0$ corresponds to a completely uncorrelated motion and $\varphi_\parallel = 1$ and $\varphi_\parallel = -1$ correspond to atomic motions perfectly in phase and out of phase, respectively.

The correlation is generally quite strong for the first coordination shell: $\varphi_\parallel \simeq 0.8$ for a number of tetrahedral semiconductors and $\varphi_\parallel \simeq 0.4$ for close-packed f.c.c. metals; the correlation is significantly weaker for the outer coordination shells and $\varphi \to 0$ when the interatomic distance increases (Fornasini & Grisenti, 2015; Jeong *et al.*, 1999).

3.4.1. Relation of the MSRD to the dynamical matrix. In the harmonic approximation, the parallel MSRD of any system can be expressed as (Crozier *et al.*, 1988)

$$\langle \Delta u_\parallel^2 \rangle = \frac{\hbar}{2\mu_{ab}} \sum_\lambda \frac{1}{\omega(\lambda)} \coth \frac{\hbar\omega(\lambda)}{2k_B T} \times \left| \left[\left(\frac{\mu_{ab}}{m_b} \right)^{1/2} \boldsymbol{\varepsilon}_b(\lambda) - \left(\frac{\mu_{ab}}{m_a} \right)^{1/2} \boldsymbol{\varepsilon}_a(\lambda) \right] \cdot \hat{\mathbf{R}} \right|^2, \quad (8)$$

where the sum is over all normal modes λ of the mass-adjusted dynamical matrix

$$D_{ab} = \frac{1}{(m_a m_b)^{1/2}} \frac{\partial^2 \mathcal{V}}{\partial \mathbf{u}_a \partial \mathbf{u}_b}, \quad (9)$$

where $\mathcal{V}$ is the total potential energy of the system, $\omega(\lambda)$ and $\boldsymbol{\varepsilon}(\lambda)$ are eigenfrequencies and normalized eigenvectors of the dynamical matrix and μ_{ab} is the reduced mass of the a–b pair.

In crystals, the translational symmetry allows one to substitute the diagonalization of the dynamical matrix (equation 9) with the diagonalization of a convenient sample of Fourier-transformed $3n \times 3n$ dynamical matrices, where n is the number of atoms per primitive cell. Accordingly,

$$\langle \Delta u_\parallel^2 \rangle = \frac{1}{\mathcal{N}} \frac{\hbar}{2\mu_{ab}} \sum_{\mathbf{q},s} \frac{1}{\omega(\mathbf{q},s)} \coth \frac{\hbar\omega(\mathbf{q},s)}{2k_B T} \times \left| \left[\left(\frac{\mu_{ab}}{m_b} \right)^{1/2} \mathbf{w}_b(\mathbf{q},s) \exp(i\mathbf{q}\cdot\mathbf{R}) - \left(\frac{\mu_{ab}}{m_a} \right)^{1/2} \mathbf{w}_a(\mathbf{q},s) \right] \cdot \hat{\mathbf{R}} \right|^2, \quad (10)$$

where the normal modes are labelled by wavevector $\mathbf{q}$ and branch index s and $\mathbf{w}(\mathbf{q},s)$ are the corresponding eigenvectors.

It is worth noting that the contribution of a pair of atoms to the MSRDs depends on the phase relations between the eigenvectors of each normal mode as well as on the projections of the eigenvector difference in the bond direction. Since different dynamical matrices can exist, sharing the same eigenfrequencies but with different eigenvectors (Cochran, 1971), the reproduction of the experimental MSRDs obtained from EXAFS represents a peculiar test for dynamical theories.

3.4.2. The Debye and Einstein models. Equations (8) and (10) are of little practical use in EXAFS analyses. The vibrational contribution to the second cumulant $C_2^* = \sigma^2(T)$ is often fitted to simple phenomenological models.

In the correlated Debye model (Beni & Platzman, 1976; Böhmer & Rabe, 1979; Sevillano *et al.*, 1979; Greegor & Lytle, 1979),

$$\sigma_{\rm D}^2(T) = \frac{3\hbar}{\omega_{\rm D}^3 m}\int_0^{\omega_{\rm D}} {\rm d}\omega\,\omega\coth\frac{\hbar\omega}{2kT}\left[1-\frac{\omega_{\rm D}\sin(\omega R q_D/\omega_{\rm D})}{\omega R q_{\rm D}}\right]. \tag{11}$$

m is the average mass of the a–b pair and the Debye frequency $\omega_{\rm D}$ is the only free parameter, corresponding to a Debye temperature $\Theta_{\rm D} = \hbar\omega_{\rm D}/k_{\rm B}$. The quantity $q_{\rm D}$ is the radius of a Debye sphere,

$$q_D = (6\pi^2/V_{\rm a})^{1/3}, \tag{12}$$

where $V_{\rm a}$ is the real-space volume per atom.

Equation (11) is an extension of the Debye model for atomic vibrations in crystallography (Willis & Pryor, 1975): the second term in square brackets takes into account the effect of correlation due to the inter-cell phase relation $\exp(i\mathbf{q}\cdot\mathbf{R})$ in equation (10). The physical significance of the correlated Debye model is more obvious for close-packed crystals with one atom per primitive cell (primitive crystals), for which the EXAFS Debye temperatures are similar for different coordination shells and are comparable to the Debye temperatures from other experimental techniques; it is questionable for non-primitive crystals (Fornasini & Grisenti, 2015).

In the Einstein model (Sevillano *et al.*, 1979) the effect of all normal modes on the absorber–backscatterer atomic pair is described in terms of a single oscillator. The Einstein expression of the parallel MSRD corresponds to the first term of equation (4) and can alternatively be expressed as

$$\begin{aligned}\sigma_{\rm E}^2(T) &= \frac{\hbar}{\mu\omega_{\rm E}}\left[\frac{1}{2}+\frac{1}{\exp(\hbar\omega_{\rm E}/kT)-1}\right]\\ &= \frac{\hbar}{2\mu\omega_{\rm E}}\coth(\hbar\omega_{\rm E}/2kT),\end{aligned} \tag{13}$$

where μ is the reduced mass of the a–b pair; the Einstein model is intrinsically correlated. The best-fitting frequencies $\omega_{\rm E} = 2\pi\nu_{\rm E}$ of different coordination shells generally differ even for primitive crystals. An effective parallel force constant $k_0 = k_\parallel = \mu\omega_{\rm E}^2$ is associated with the frequency $\omega_{\rm E} = \omega_\parallel$, which represents a measure of the effective interaction strength.

At high temperatures $\sigma_{\rm E}^2 \to kT/\mu\omega_{\rm E}^2$ (the classical approximation). For $T = 0$, $\sigma_{\rm E}^2 = \sigma_0^2 = \hbar/2\mu\omega_{\rm E}$ (the zero-point contribution). The Einstein model best fitting the second cumulant of the first shell of copper in shown in Fig. 1 together with the corresponding classical approximation.

The Debye and Einstein models are useful to parametrize the vibrational contribution to the MSRD of a given atomic pair. Besides, deviations of experimental MSRD values from the models are helpful in detecting different contributions to disorder. Temperature-independent structural disorder, for example due to distorted coordination shells, generally leads to a constant positive contribution to the MSRD in addition to the temperature-dependent value of the vibrational models. Deviations of the temperature dependence from that of the vibrational models can suggest the presence of phase transitions or of temperature-dependent structural disorder.

3.5. Anharmonicity effects

The third and fourth cumulants obtained from the EXAFS analysis of many-atomic systems can be fitted by the one-dimensional models presented in Section 3.2. In Fig. 1, the quantum and classical models that best fit the third cumulant of the first shell of copper are shown.

If the third and fourth cumulants are measured as a function of temperature with sufficient accuracy, one can separate the harmonic and anharmonic contributions to the second cumulant (parallel MSRD) corresponding to the first and the other terms of equation (4), respectively. The effect of anharmonicity is a progressive decrease in the frequency of relative vibrations when the temperature increases. From the logarithmic derivative of the frequency with respect to the bond expansion, a constant-pressure bond Grüneisen parameter (GP) $\gamma_{{\rm b},p}$ has been evaluated for CdTe (Fornasini & Grisenti, 2015). From pressure-dependent EXAFS measurements on CdTe, a constant-temperature bond GP $\gamma_{{\rm b},T}$ has been obtained and found to be significantly smaller than $\gamma_{{\rm b},p}$ (Fornasini *et al.*, 2018).

3.6. Bond distance and bond expansion

The inadequacy of the one-dimensional model in dealing with many-atomic systems mainly affects the interatomic distance and thermal expansion. The first EXAFS cumulant directly measures the average interatomic distance (the bond distance for the first coordination shell) and is connected to the distance R between the average atomic positions, as measured by Bragg scattering, by (Lagarde, 1985; Dalba *et al.*, 1995; Stern, 1997)

$$C_1^* = \langle r\rangle \simeq R + \langle\Delta u_\perp^2\rangle/2R. \tag{14}$$

The bond distance $\langle r\rangle$ is larger than the crystallographic distance R owing to the effect of perpendicular vibrations (Busing & Levy, 1964; Willis & Pryor, 1975). Accurate EXAFS measurements of the bond expansion $\delta C_1^* = \delta\langle r\rangle$ are now routinely performed (Filipponi & Di Cicco, 1995; Dalba *et al.*, 1999; Yokoyama & Eguchi, 2011). In some cases, it has been possible to evaluate the temperature dependence of the coefficient of bond expansion (Fornasini & Grisenti, 2014). For a review, see Fornasini *et al.* (2017) and references therein.

For many-atomic systems the bond expansion δC_1^* is different from the quantity a defined in equation (7): the bond expansion cannot be accounted for solely by the anharmonicity of the effective pair potential energy, and an additional temperature dependence of the minimum position of the effective pair potential energy has to be considered. Such a potential shift has been detected experimentally and has been confirmed by theoretical simulations (a Beccara & Fornasini, 2008; Sanson, 2010). To summarize, in diatomic molecules the bond expansion $\delta\langle r\rangle$ is completely determined by the distribution asymmetry, while in many-atomic systems the contributions of asymmetry and potential shift are comparable for nearest-neighbour distances and the potential shift neatly prevails for outer-shell distances.

3.7. Perpendicular MSRD

The perpendicular MSRD $\langle \Delta u_\perp^2 \rangle$ can be calculated by inverting equation (14), provided that R is known from Bragg scattering measurements and assuming that the vibrations are isotropic within the plane perpendicular to the bond. Correlated Debye and Einstein models can be fitted to the perpendicular MSRD (Vaccari & Fornasini, 2006). The parallel and perpendicular Debye or Einstein frequencies are generally different. The perpendicular Einstein frequency can be connected to an effective perpendicular force constant $k_\perp = \mu(\omega_\perp)^2$. The parallel and perpendicular effective force constants $k_\parallel$ and $k_\perp$ should not be confused with the force constants of lattice dynamical models; for a discussion, see Abd el All *et al.* (2012).

In general, the degree of correlation is different for parallel and perpendicular MSRDs; as a consequence, the ellipsoids of relative absorber–backscatterer motion are generally anisotropic, even when the thermal ellipsoids of single atoms are isotropic. A measure of anisotropy is given by the ratio of the parallel to perpendicular effective force constants, $\xi = (k_\parallel/k_\perp)^{1/2}$. For perfectly isotropic relative vibrations $\xi = 1$. The anisotropy is very weak for the close-packed structure of copper ($\xi \simeq 1.08$). For a number of tetrahedral semiconductors, ξ values of between 1.7 and 2.46 have been found; larger degrees of anisotropy have been found in some framework structures. For a review, see Fornasini *et al.* (2017).

4. Theoretical approaches

4.1. Quantum statistical methods

Quantum statistical methods can be considered as an extension of the procedures developed for the one-dimensional model to many-atomic systems. They can rely on perturbative approaches, which are suitable for weak anharmonicity, or on effective potential path-integral approaches, which are suitable for strong anharmonicity.

In Fujikawa & Miyanaga (1993) a general method is presented for calculating the first four cumulants in the plane-wave approximation in terms of eigenfrequencies and eigenvectors of normal modes. The method is based on the finite-temperature many-body perturbation theory for anharmonic crystals by use of the temperature Green's function (Barron & Klein, 1974). Taking into account cubic and quartic anharmonicity, some general qualitative properties of cumulants are obtained. The method was applied to monatomic and diatomic one-dimensional chains in Miyanaga & Fujikawa (1994), where the nearest-neighbour interaction is described by a Morse potential whose power expansion is limited to the quartic term. Some attempts have also been performed for f.c.c. crystals (Katsumata *et al.*, 2001).

For strongly anharmonic systems, a real-space approach based on the finite-temperature path-integral method (Feynman, 1972) has been developed (Fujikawa *et al.*, 1997), in which by introducing a local effective potential that takes into account quantum fluctuations, a classical-like connection is established between potential energy and distance distribution. This method has been applied to asymmetric double-well potentials by Nitta *et al.* (2006).

4.2. Phenomenological approaches

Using a simpler phenomenological approach, Van Hung & Rehr (1997) derived an anharmonic correlated model for the effective potential, taking into account the interaction of absorber and backscatterer atoms with their nearest neighbours via a Morse potential; the method was applied to calculations for copper and nickel (Van Hung & Fornasini, 2007) and for zinc and cadmium (Van Hung, Tien *et al.*, 2014), and was extended to silicon and germanium using Stillinger–Weber potentials (Van Hung, Thang *et al.*, 2014).

4.3. Molecular-dynamics and Monte Carlo approaches

The cumulants can be evaluated by sampling a configurational space obtained by molecular-dynamics (MD) or Monte Carlo (MC) sampling. MC simulations based on empirical pair potentials have been performed by Yokoyama *et al.* (1997) on solid krypton in the temperature range 24–43 K. Classical MD based on empirical pair potentials has been used by Edwards *et al.* (1997) to calculate the cumulants of copper and by Sanson to calculate the cumulants of germanium (Sanson, 2010) and of CdSe (Sanson, 2011). Classical MD and MC simulations cannot reproduce the low-temperature quantum behaviour of cumulants. To overcome this difficulty, a Beccara and coworkers (a Beccara *et al.*, 2003; a Beccara & Fornasini, 2008) performed path-integral Monte Carlo (PIMC) sampling of the thermal configurations of copper. PIMC sampling is based on the sampling of the thermal density matrix after it has been transformed into the convolution of P matrices each with an effective temperature P times higher, corresponding to P copies of the system linked together by a harmonic potential. The resulting probability distribution is sampled by means of appropriate generalized Metropolis algorithms. For the first shell, very good agreement was obtained with the experimental bond expansion and third cumulant as well as the parallel and perpendicular MSRDs. Beyond the first shell, where the analysis of experimental data is severely limited by MS effects, PIMC simulations allowed the independent determination of the bond thermal expansion, of the shift of the maximum of the distribution of distances and of the third cumulant.

4.4. Equation of motion

An approach for calculating the Debye–Waller (DW) factors in the harmonic approximation for aperiodic systems has been proposed by Poiarkova & Rehr (1999) based on the equation of motion (EM) method, which involves a Fourier transform of the time dependence of the molecular dynamics. The approach has been used to calculate the DW factor of multiple-scattering (MS) paths in a 459-atom spherical cluster of copper, in a 147-atom spherical cluster of germanium and in the complex organic structure of zinc tetraimidazole. In all cases, valence force-field (VFF) models were chosen to parametrize the interaction potential energy.

4.5. *Ab initio* calculations

Ab initio calculations based on density-functional theory (DFT) have been performed for several molecules by Dimakis & Bunker (1998, 2006). A first-principles approach to calculate the force constants for various systems within the quasi-harmonic approximation using DFT has been developed by Vila *et al.* (2007), who critically compared different approximations of the exchange–correlation potential. A good agreement with available experimental data has been found for the parallel MSRD of the first four shells of copper, germanium and GaAs, as well as for the first-shell perpendicular MSRD, the bond expansion and the third cumulant of copper. The ratio of perpendicular to parallel MSRD has also been found to be in agreement with the experimental value for germanium. An *ab initio* EM approach has been developed by Vila *et al.* (2012) to evaluate the DW factors while avoiding the explicit calculation of phonon modes. The method is based on DFT MD calculations of displacement–displacement time-correlation functions.

References

Abd el All, N., Dalba, G., Diop, D., Fornasini, P., Grisenti, R., Mathon, O., Rocca, F., Thiodjio Sendja, B. & Vaccari, M. (2012). *J. Phys. Condens. Matter*, **24**, 115403.

a Beccara, S., Dalba, G., Fornasini, P., Grisenti, R., Pederiva, F., Sanson, A., Diop, D. & Rocca, F. (2003). *Phys. Rev. B*, **68**, 140301.

a Beccara, S. & Fornasini, P. (2008). *Phys. Rev. B*, **77**, 172304.

Alberding, N. & Crozier, E. D. (1983). *Phys. Rev. B*, **27**, 3374–3382.

Ashley, C. A. & Doniach, S. (1975). *Phys. Rev. B*, **11**, 1279–1288.

Barron, T. H. K. & Klein, M. L. (1974). *Dynamical Properties of Solids*, Vol. 1, edited by G. K. Horton & A. A. Maradudin, pp. 391–450. Amsterdam: North-Holland.

Benfatto, M., Natoli, C. R. & Filipponi, A. (1989). *Phys. Rev. B*, **40**, 9626–9635.

Beni, G. & Platzman, P. M. (1976). *Phys. Rev. B*, **14**, 1514–1518.

Böhmer, W. & Rabe, P. (1979). *J. Phys. C Solid State Phys.* **12**, 2465–2474.

Boland, J. J. & Baldeschwieler, J. D. (1984). *J. Chem. Phys.* **80**, 3005–3015.

Booth, C. H., Bridges, F., Bauer, E. D., Li, G. G., Boyce, J. B., Claeson, T., Chu, C. W. & Xiong, Q. (1995). *Phys. Rev. B*, **52**, R15745–R15748.

Boyce, J. B., Hayes, T. M., Stutius, W. & Mikkelsen, J. C. Jr (1977). *Phys. Rev. Lett.* **38**, 1362–1365.

Brouder, C. (1988). *J. Phys. C Solid State Phys.* **21**, 5075–5086.

Bunker, G. (1983). *Nucl. Instrum. Methods Phys. Res.* **207**, 437–444.

Bunker, G. (2010). *Introduction to XAFS.* Cambridge University Press.

Busing, W. R. & Levy, H. A. (1964). *Acta Cryst.* **17**, 142–146.

Cochran, W. (1971). *Acta Cryst.* A**27**, 556–559.

Crozier, E. D., Rehr, J. J. & Ingalls, R. (1988). *X-ray Absorption*, edited by D. C. Koningsberger & R. Prins, pp. 373–442. New York: John Wiley & Sons.

Crozier, E. D. & Seary, A. J. (1980). *Can. J. Phys.* **58**, 1388–1399.

Dalba, G. & Fornasini, P. (1997). *J. Synchrotron Rad.* **4**, 243–255.

Dalba, G., Fornasini, P., Gotter, R. & Rocca, F. (1995). *Phys. Rev. B*, **52**, 149–157.

Dalba, G., Fornasini, P., Grisenti, R. & Purans, J. (1999). *Phys. Rev. Lett.* **82**, 4240–4243.

Dimakis, N. & Bunker, G. (1998). *Phys. Rev. B*, **58**, 2467–2475.

Dimakis, N. & Bunker, G. (2006). *Biophys. J.* **91**, L87–L89.

Edwards, A. B., Tildesley, D. J. & Binsted, N. (1997). *Mol. Phys.* **91**, 357–369.

Eisenberger, P. & Brown, G. S. (1979). *Solid State Commun.* **29**, 481–484.

Feynman, R. P. (1972). *Statistical Mechanics.* Reading: Benjamin.

Filipponi, A. & Di Cicco, A. (1995). *Phys. Rev. B*, **51**, 12322–12336.

Fornasini, P. (2024). *Int. Tables Crystallogr. I*, ch. 5.11, 683–686.

Fornasini, P., a Beccara, S., Dalba, G., Grisenti, R., Sanson, A., Vaccari, M. & Rocca, F. (2004). *Phys. Rev. B*, **70**, 174301.

Fornasini, P. & Grisenti, R. (2014). *J. Chem. Phys.* **141**, 164503.

Fornasini, P. & Grisenti, R. (2015). *J. Synchrotron Rad.* **22**, 1242–1257.

Fornasini, P., Grisenti, R., Dapiaggi, M., Agostini, G. & Miyanaga, T. (2017). *J. Chem. Phys.* **147**, 044503.

Fornasini, P., Grisenti, R., Irifune, T., Shinmei, T., Mathon, O., Pascarelli, S. & Rosa, A. D. (2018). *J. Phys. Condens. Matter*, **30**, 245402.

Fornasini, P., Monti, F. & Sanson, A. (2001). *J. Synchrotron Rad.* **8**, 1214–1220.

Frenkel, A. I. & Rehr, J. J. (1993). *Phys. Rev. B*, **48**, 585–588.

Fujikawa, T. & Miyanaga, T. (1993). *J. Phys. Soc. Jpn*, **62**, 4108–4122.

Fujikawa, T., Miyanaga, T. & Suzuki, T. (1997). *J. Phys. Soc. Jpn*, **66**, 2897–2906.

Greegor, R. B. & Lytle, F. W. (1979). *Phys. Rev. B*, **20**, 4902–4907.

Gurman, S. J. & Pendry, J. B. (1976). *Solid State Commun.* **20**, 287–290.

Haug, J., Chassé, A., Schneider, R., Kruth, H. & Dubiel, M. (2008). *Phys. Rev. B*, **77**, 184115.

Huber, K. P. & Herzberg, G. (1979). *Molecular Spectra and Molecular Structure IV: Constants of Diatomic Molecules.* New York: Van Nostrand Reinhold.

Jeong, I. K., Proffen, T., Mohiuddin-Jacobs, F. & Billinge, S. J. L. (1999). *J. Phys. Chem. A*, **103**, 921–924.

Katsumata, H., Miyanaga, T., Yokoyama, T., Fujikawa, T. & Ohta, T. (2001). *J. Synchrotron Rad.* **8**, 226–228.

Lagarde, P. (1985). *Amorphous Solids and the Liquid State*, edited by N. H. March, R. A. Street & M. Tosi, pp. 365–394. New York: Plenum Press.

Lee, P. A. & Pendry, J. B. (1975). *Phys. Rev. B*, **11**, 2795–2811.

Loeffen, P. W. & Pettifer, R. F. (1996). *Phys. Rev. Lett.* **76**, 636–639.

Miyanaga, T. & Fujikawa, T. (1994). *J. Phys. Soc. Jpn*, **63**, 1036–1052.

Mustre de Leon, J., Conradson, S. D., Batistić, I., Bishop, A. R., Raistrick, I. D., Aronson, M. C. & Garzon, F. H. (1992). *Phys. Rev. B*, **45**, 2447–2457.

Nitta, K., Miyanaga, T. & Fujikawa, T. (2006). *J. Phys. Soc. Jpn*, **75**, 054603.

Poiarkova, A. V. & Rehr, J. J. (1999). *Phys. Rev. B*, **59**, 948–957.

Rehr, J. J. & Albers, R. C. (2000). *Rev. Mod. Phys.* **72**, 621–654.

Sanson, A. (2010). *Phys. Rev. B*, **81**, 012304.

Sanson, A. (2011). *J. Phys. Condens. Matter*, **23**, 315401.

Sayers, D. E., Stern, E. A. & Lytle, F. W. (1971). *Phys. Rev. Lett.* **27**, 1204–1207.

Sevillano, E., Meuth, H. & Rehr, J. J. (1979). *Phys. Rev. B*, **20**, 4908–4911.

Stern, E. A. (1997). *J. Phys. IV Fr.* **7**, 137–140.

Stern, E. A., Bunker, B. A. & Heald, S. M. (1980). *Phys. Rev. B*, **21**, 5521–5539.

Stern, E. A., Heald, S. M. & Bunker, B. (1979). *Phys. Rev. Lett.* **42**, 1372–1375.

Stern, E. A., Līvņš, P. & Zhang, Z. (1991). *Phys. Rev. B*, **43**, 8850–8860.

Stern, E. A., Sayers, D. E. & Lytle, F. W. (1975). *Phys. Rev. B*, **11**, 4836–4846.

Tranquada, J. M. & Ingalls, R. (1983). *Phys. Rev. B*, **28**, 3520–3528.

Vaccari, M. & Fornasini, P. (2006). *J. Synchrotron Rad.* **13**, 321–325.

Van Hung, N. & Fornasini, P. (2007). *J. Phys. Soc. Jpn*, **76**, 084601.

Van Hung, N. & Rehr, J. J. (1997). *Phys. Rev. B*, **56**, 43–46.

Van Hung, N., Thang, C. S., Toan, N. C. & Hieu, H. K. (2014). *Vacuum*, **101**, 63–66.
Van Hung, N., Tien, T. S., Duc, N. B. & Vuong, D. Q. (2014). *Mod. Phys. Lett. B*, **28**, 1450174.
Vila, F. D., Lindahl, V. E. & Rehr, J. J. (2012). *Phys. Rev. B*, **85**, 024303.
Vila, F. D., Rehr, J. J., Rossner, H. H. & Krappe, H. J. (2007). *Phys. Rev. B*, **76**, 014301.
Willis, B. T. M. & Pryor, A. W. (1975). *Thermal Vibrations in Crystallography*. Cambridge University Press.
Yokoyama, T. (1999). *J. Synchrotron Rad.* **6**, 323–325.
Yokoyama, T. & Eguchi, K. (2011). *Phys. Rev. Lett.* **107**, 065901.
Yokoyama, T., Kobayashi, K., Ohta, T. & Ugawa, A. (1996). *Phys. Rev. B*, **53**, 6111–6122.
Yokoyama, T., Ohta, T. & Sato, H. (1997). *Phys. Rev. B*, **55**, 11320–11329.